Journal of CO2 Utilization 86 (2024) 102897

Contents lists available at ScienceDirect

Journal of CO2 Utilization

journal homepage: www.elsevier.com/locate/jcou

# Inhibiting salt precipitation on the gas diffusion electrode surface in gas-phase $CO_2$ electroreduction to formate by using an acidic anolyte

Jose Antonio Abarca *, Guillermo Díaz-Sainz *, Angel Irabien

*Departamento de Ingenierías Química y Biomolecular, Universidad de Cantabria, Avenida de los Castros s/n, Santander 39005, Spain*

ARTICLE INFO

*Keywords:*
Gas-phase $CO_2$ electroreduction
Formate
GDE stability
Acid anolyte
Salt precipitation

ABSTRACT

The gas-phase $CO_2$ electroreduction to formate represents one of the most promising $CO_2$ conversion processes due to its scalability, as the product concentration surpasses 30 % wt. However, the use of alkaline media anolytes, intended to improve the efficiency and selectivity of formate production, causes the carbonate and bicarbonate salts to precipitate over the Gas Diffusion Electrode (GDE). This precipitation clogs the porous structure, leading to a rapid loss of electrode stability. In this work, we address this issue by proposing the use of acid anolytes, based on $K_2SO_4$, to mitigate the precipitation of insoluble salt on the GDE structure, thereby achieving longer and more stable GDE operation times. Various anolyte concentrations and pHs are evaluated, with 0.3 M $K_2SO_4$ at pH 1, adjusted using $H_2SO_4$, providing the best compromise. This condition inhibited potassium carbonate and bicarbonate precipitation, as observed through XRD, SEM, and EDS analysis, while maintaining high $CO_2$ electroreduction to formate performance, with a concentration of 69 g $L^{-1}$, and a Faradaic Efficiency of 33 %. Furthermore, the anolyte flowrate per geometric area is optimized to maximize the system performance. At a flowrate of 0.85 mL $min^{-1}$ $cm^{-2}$, enhanced concentration of 88 g $L^{-1}$ and a Faradaic Efficiency of 42 % are reached. Besides, long-term experiments demonstrated that GDEs used with alkaline conditions exhibit a larger deactivation constant (0.7652) compared to the GDEs used with acid anolytes (0.3891). This indicates that salt precipitation more rapidly reduces GDE performance under alkaline conditions. These results represent a promising advance in obtaining longer-lasting GDEs, which are crucial to successfully scaling up the $CO_2$ electroreduction to formate.

## 1. Introduction

Global warming and climate change have emerged as significant concerns in recent years, representing some of the most pressing challenges facing society today. The rise in the concentration of carbon dioxide ($CO_2$) in the atmosphere stands out as a primary factor driving the Earth's rising temperature. $CO_2$ emissions originate from a diverse array of sources, predominantly from human activities such as energy generation, mobility and industrial sectors [1]. Consequently, the pursuit of various strategies to mitigate these emissions has taken center stage in global discussions, with the latest United Nations Climate Change Conference of the Parties (COP28) aiming to establish a society emitting zero net $CO_2$ by 2050 [2].

In this context, the development of Carbon Capture, Utilization, and Storage (CCUS) technologies has garnered significant attention as one of the most promising strategies for curbing industrial $CO_2$ emissions [3]. Among these alternatives, $CO_2$ electroreduction stands out as an effective means of recycling $CO_2$ into valuable products through the application of an external voltage. This process fosters sustainability in industrial processes by adopting a circular economy model that repurposes $CO_2$ as an alternative raw material [4,5]. Besides, the electrocatalytic $CO_2$ conversion holds promise for storing energy from intermittent renewable sources in the form of chemical bonds [6].

Different chemical products can be derived from direct electroconversion of $CO_2$, including formate ($HCOO^-$), formic acid (HCOOH), methane ($CH_4$), methanol ($CH_3OH$) carbon monoxide (CO), ethanol ($CH_3CH_2OH$), ethylene ($C_2H_4$), among others. Among these, formate is particularly noteworthy as one of the most promising products nearing industrial-scale implementation in $CO_2$ electroreduction [7]. Significant progress has been made in recent years in $CO_2$ electroreduction to formate, driven by progress in catalyst selection [8–10], reactor configuration [11–13], electrode fabrication [14,15], and operational conditions [16,17]. These advancements have culminated in achieving high Faradaic Efficiencies (FE) ranging between 80 % and 90 % in

* Corresponding authors.
*E-mail addresses:* joseantonio.abarca@unican.es (J.A. Abarca), diazsg@unican.es (G. Díaz-Sainz).

https://doi.org/10.1016/j.jcou.2024.102897
Received 21 June 2024; Received in revised form 26 July 2024; Accepted 6 August 2024
Available online 10 August 2024

formate production, product concentrations over 35 % wt, and energy consumptions lower than 200 kWh $kmol^{-1}$ of formate [5].

Several reactor configurations have been proposed for $CO_2$ electroreduction to formate. However, continuous electrochemical cells offer numerous advantages for industrial applications [18]. Among these, gas-liquid (G-L) continuous operation, in which the cathode feed is gaseous $CO_2$ that reacts at the gas-liquid-solid phase boundary. This boundary is formed by the close contact between the ion exchange membrane and the electrode surface, where the $CO_2$ reduction to formate takes place. This configuration. simplified as gas-phase operation, has emerged as one of the most effective operational configurations for achieving the target product concentration of 85 % wt. for the industrial production of formate via $CO_2$ electroreduction [16]. In this setup, a liquid anolyte, as the liquid phase, is usually delivered to the anode, while a humidified $CO_2$ stream, as the gas phase, is directed to the cathode. The cathode configuration employed in this setup is a Gas Diffusion Electrode (GDE). The porous structure of the GDE facilitates the passage of $CO_2$ to reach the catalyst surface, where the reduction reaction occurs at the three-phase boundary (gas-liquid-solid) (G-L-S) [19]. GDEs typically consist of a porous carbonaceous support, often carbon paper, a microporous layer to enhance $CO_2$ mass transfer, and a catalytic layer where the reaction takes place [20].

On the other hand, an alkaline solution is commonly employed as the anolyte in the anode compartment to suppress the competitive Hydrogen Evolution Reaction (HER) during $CO_2$ reduction to formate [21]. The reaction mechanism for $CO_2$ electroreduction to formate under alkaline conditions is described in Eq. 1 [22]:

$$CO_2 + H_2O + 2e^- \rightarrow HCOO^- + OH^- \quad (1)$$

However, due to the formation of hydroxide anion radicals, local alkaline conditions at the reaction sites promote the reaction of $CO_2$ with hydroxide ($OH^-$), yielding carbonates ($CO_3^{2-}$) and bicarbonates ($HCO_3^-$) as depicted in Eqs. 2 and 3 [5]:

$$CO_2 + OH^- \rightarrow HCO_3^- \quad (2)$$

$$HCO_3^- + OH^- \rightarrow CO_3^{2-} + H_2O \quad (3)$$

While KOH, $KHCO_3$, and $K_2SO_4$ are commonly used as anolyte solutions in $CO_2$ electroreduction to formate [5], alkaline hydroxide solutions, particularly KOH, NaOH, or CsOH, are preferred, as they enhance $CO_2$ electroreduction kinetics, resulting in higher current densities compared to neutral anolytes (such as $KHCO_3$ or $K_2SO_4$) at the same potential applied [23]. Additionally, hydroxide anolytes typically contain high concentrations of metal cations ($K^+$, $Na^+$, or $Cs^+$). These cations permeate through the ion exchange membrane, leading to the formation of insoluble salts (carbonate and bicarbonates) at the cathode, which is the primary mechanism for GDE deactivation [24]. Table 1 summarizes the solubilities of some of the most common salts formed.

The absence of a liquid catholyte accelerates the precipitation of these salts on the GDE surface, covering a significant portion of its active area. A schematic illustration of this salt precipitation mechanism is presented in Fig. 1:

As depicted in Fig. 1, the precipitation of significant amounts of insoluble salts obstructs the porous structure of the GDE. This obstruction hinders the passage of $CO_2$ feed to reach the catalyst's active sites within the catalyst layer adjacent to the ion exchange membrane. Consequently, $CO_2$ encounters limited access to the catalyst, and the external overpotential provided to the system is diverted towards other competitive electrochemical reactions, notably the HER, which significantly reduces the FE towards formate [25,26]. Moreover, the hydrophilic nature of carbonate and bicarbonate salts can alter the overall hydrophobicity of the GDE, crucial for preventing electrode flooding. Salt precipitation affects the capillarity of the pores in the GDE, leading to flooding and increasing the $CO_2$ mass transfer resistance, further disadvantaging $CO_2$ electroreduction to formate compared to the HER [27]. Both mechanisms of GDE deactivation predominantly occur at high current densities, where rapid (bi)carbonate leads to the swift deactivation of the electrode. Therefore, developing strategies focused on mitigating salt precipitation on the GDE is essential for enabling long-term and stable operation of gas-phase $CO_2$ electroreduction to formate at high current densities for industrial scaling-up [28].

Numerous strategies have been explored to mitigate the impact of salt accumulation on GDEs. These strategies may target material properties or reactor operational conditions [24]. Operationally, some strategies focus on the $CO_2$ feed stream, such as $CO_2$ humidification to maintain membrane and cathode surface humidity. Wheeler et al. [29] propose that a dry cathode condition increases the water and ion flux from the anode compartment through the membrane, resulting in more salt formation at the cathode. Therefore, ensuring some level of humidity in the $CO_2$ feed can delay salt crystal formation [29,30]. Other strategies involve regulating gas flow rate or temperature [31], although these approaches may not be practical for industrial-level operations. Additionally, salt precipitates can be periodically removed by flushing them out of the GDE [30–32]. However, this removal process may pose challenges for certain reactor geometries, particularly in flow field reactors.

Employing distinct strategies tailored to the various materials and components of an electrochemical reactor can effectively mitigate salt precipitation. Among these components, the membrane's properties hold particular significance. Cation exchange membranes (CEM) facilitate the passage of metal alkali cations from the anode to the cathode, thereby contributing to undesirable salt precipitation [16]. Conversely, anion exchange membranes (AEM) hinder cation migration toward the cathode [33]. Nonetheless, formate anions may still traverse these membranes to the anode, where they undergo reoxidation, leading to decreased system efficiency. Bipolar membranes (BPMs) present a promising solution to various $CO_2$ electrolysis challenges, including salt formation and precipitation. Comprising an anion exchange layer (AEL) and a cation exchange layer (CEL), BPMs, when operated under reverse bias, can split water, directing protons to the cathode and hydroxides to the anode [34]. This process facilitates the direct production of formic acid, thereby mitigating salt formation on the GDE. However, the water dissociation reaction can significantly increase cell ohmic resistance, thereby limiting operation at high current densities.

Another critical aspect influencing the gas-phase $CO_2$ electroreduction is the composition and pH of the anolyte solution. As aforementioned, the use of alkaline solutions promotes formate production over HER but accelerates salt precipitation, and accelerates GDE deactivation [5]. Investigations have explored alternatives such as employing anolytes with metal cations forming highly soluble (bi)carbonates, like $Cs^+$ [23], or incorporating divalent cation salts in the anolyte formulation [35]. However, these approaches only delay rather than prevent salt precipitation, and salt precipitation continues to degrade GDE performance. Another alternative involves using an acidic medium as the anolyte, potentially avoiding completely the precipitation of salts [36]. However, precise control of pH and conductivity is imperative in such cases to prevent HER promotion [37]. Acidic anolytes, rich in protons, can hinder the combination of reaction intermediates in $CO_2$ electroreduction with metal cations, thus effectively inhibiting salt precipitation by reducing (bi)carbonate formation [38]. To the best of the authors' knowledge, different studies have implemented the use of

**Table 1**
Molar solubility of different metal alkali cation carbonate and bicarbonates in water under standard conditions (25 ºC and 1 atm). Table adapted from reference [24].

| Alkali metal cation | Bicarbonate solubility ($HCO_3^-$) (M) | Carbonate solubility ($CO_3^{2-}$) (M) |
|---|---|---|
| $Na^+$ | 1.23 | 2.90 |
| $K^+$ | 3.62 | 8.03 |
| $Cs^+$ | 10.78 | 8.01 |

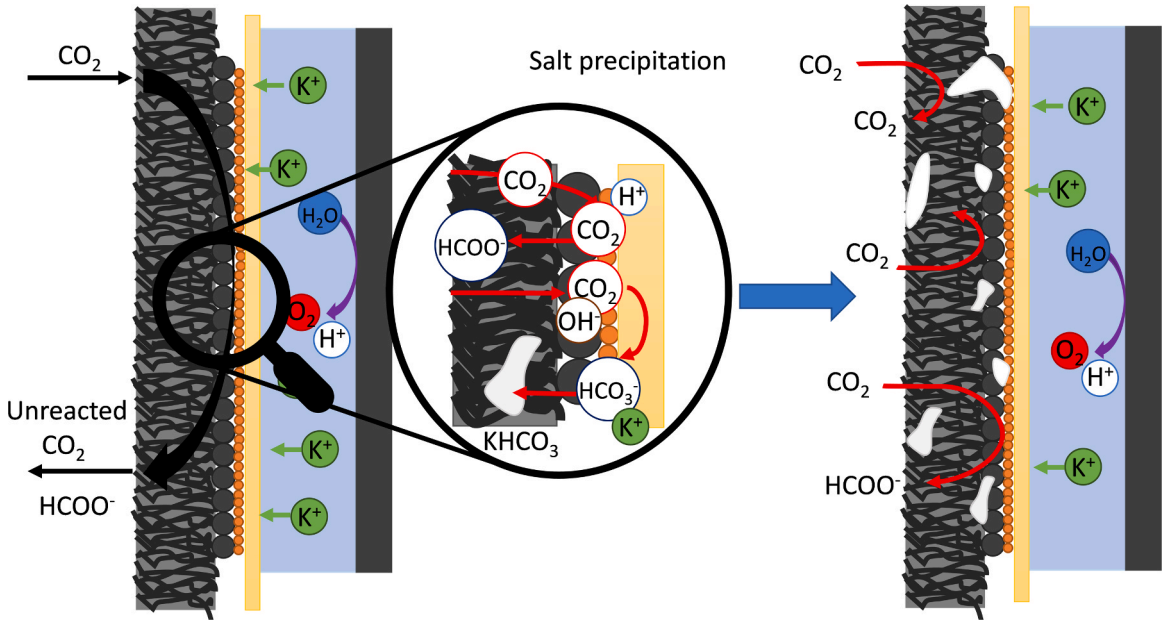


**Fig. 1.** Schematic representation of the mechanism of $CO_2$ electroreduction to formate, along with the formation and precipitation of (bi)carbonates formation over the GDE structure during gas-phase $CO_2$ electroreduction to formate, using KOH as an example of an anolyte.

acid anolytes for gas-phase $CO_2$ electroreduction to different products, such as CO, however, no studies have successfully utilized acidic anolytes in gas-phase $CO_2$ electroreduction to formate.

The primary objective of this work is to explore the viability of using an acidic anolyte, composed of aqueous $K_2SO_4$ solutions with pH adjustment, to mitigate salt precipitation on the GDE during gas-phase $CO_2$ electroreduction for formate production. To achieve this objective, a bismuth-based catalyst is used due to its previously demonstrated high selectivity towards formate [39]. The study assesses the composition of the anolyte, pH levels, and flowrates to optimize formate production while preventing salt precipitation on the cathode. Various figures of merit including FE, formate rate, energy consumption, and the quantity of (bi)carbonates formed on the cathode, are analyzed, additionally, the loss of activity of the GDE is evaluated by estimating a first-order deactivation constant during 5 h stability tests. Moreover, physicochemical characterization of the GDEs is conducted to evaluate the impact of reaction conditions on their structure and potential deactivation. The findings of this investigation hold promise for addressing GDE deactivation issues resulting from salt precipitation, thereby enabling prolonged operation of gas-phase $CO_2$ electroreduction for formate production, which is crucial for process scalability.

## 2. Methodology

### 2.1. GDE fabrication

A bismuth-based GDE was chosen for conducting the electrochemical $CO_2$ reduction to formate. This electrode comprises Toray TGP-H-60 carbon paper (Alfa Aesar) as the carbonaceous support, with a catalytic layer deposited onto the support using an optimized automatic spray pyrolysis technique, as detailed in previous studies [15]. The catalytic ink, sprayed onto the support, consists of 150 mg of commercial $Bi_2O_3$ (Sigma Aldrich, 90–210 nm), 150 mg of Vulcan XC-72R (Cabot), 375 mg of PTFE (60 % wt. Sigma Aldrich), and 1285 mg of 5 % wt. Nafion D521 suspension (Ion Power), dissolved in 25 mL of ethanol (96 % wt. Scharlau) as the solvent. Before electrode fabrication, the ink undergoes sonication for 1 hour to ensure complete suspension of the catalytic material.

The resulting GDEs have a geometrical area of 10 $cm^2$, with a catalyst loading of 4 mg $cm^{-2}$. Following the application of the catalytic ink, the GDEs are dried in an oven at 80 °C for 1 hour. Subsequently, they undergo activation in a 1 M HCl acidic solution for 45 minutes, followed by air-drying.

### 2.2. Experimental set up

The $CO_2$ electroreduction process to formate is conducted in a filter-press electrochemical reactor (ElectroCell). The system enables a single pass of the reactants and is configured for gas-phase operation, as shown in Figure S.1. A humified $CO_2$ stream is directed to the cathode compartment at a flow rate of 200 mL $min^{-1}$. The ion exchange membrane used in this setup is a Nafion-117 (Ion Power) CEM, activated in HCl 1 M. The GDE is positioned in contact with the membrane. A magnetically stirred glass tank serves as a reservoir for the anolyte solution, comprised of $K_2SO_4$ (PanReac AppliChem) and $H_2SO_4$ (96 % wt. PanReac AppliChem) for pH adjustment. The flow rate to the system, ranging between 0.14 and 1.71 mL $min^{-1}$ $cm^{-2}$, is controlled by a peristaltic pump (HygiaFlex). The system uses a dimensionally stable anode, DSA/$O_2$ (Ir-MMO mixed metal oxide on platinum). To ensure proper wetting, a leak-free Ag/AgCl 3.4 M KCl reference electrode is placed within a PTFE frame in the anode compartment.

The experiments are conducted under galvanostatic conditions, maintaining a constant current density of 200 mA $cm^{-2}$, regulated by a potentiostat-galvanostat (Arbin Instruments, MSTT4). Each experiment spans 60 minutes, with a single liquid-product sample collected at the end of each run. Gas-product measurements are conducted at 5-minute intervals during experiments where applicable. Each experiment is replicated at least twice.

Formate concentration in the liquid samples is determined using liquid ion chromatography (Dionex ICS 1100, equipped with an AS9-HC column). Carbonate and bicarbonate titration is performed against 0.01 N HCl (PanReac AppliChem) using Phenolphthalein (1 % PanReac AppliChem), and methyl orange (0.04 % PanReac AppliChem) as indicators, respectively. Gas-product quantification is facilitated by a gas-chromatographer (990 MicroGC, Agilent Technologies) connected to the system's output during experiments.

### 2.3. Experimental conditions for the acid anolyte

The evaluation of different parameters of the acid anolyte on the

performance of gas-phase $CO_2$ electroreduction to formate is conducted. Initially, the composition of the anolyte is examined, varying the concentration of $K_2SO_4$ within the range of 0.1–0.5 M while maintaining a constant pH value of 2. Once an optimal anolyte composition, balancing salt precipitation reduction and formate efficiency maximization is identified, different pH values of the anolyte ranging from 1 to 4 are assessed. Subsequently, for the identified optimal anolyte concentration and pH, the influence of the inlet flowrate is investigated, operating within flow rate ranges of 0.14–1.71 mL $min^{-1}$ $cm^{-2}$. A summary of the different experimental conditions is presented in Table 2.

### 2.4. GDE physicochemical characterization

Following each experiment, the GDEs undergo characterization to assess the impact of salt precipitation on their structures. Fresh GDEs are also characterized to compare with the physicochemical features of the used ones under different experimental conditions. Different techniques are employed for this purpose.

Salt precipitation over the GDE surface is determined by evaluating the crystallinity and composition of the electrode surface using X-ray diffraction (XRD). Spectra from different samples are obtained using a Bruker D8 ADVANCE diffractometer operating at 40 kV and 25 mA. Measurements are performed between 0 and 100° employing a Cu X-ray tube (Cu-Kα) as the emission source.

Microstructure alterations of the GDEs are analyzed by Scanning electron microscopy (SEM), utilizing a Zeiss EVO MA 15 scanning field emission microscope equipped with a Schottky-type gun, secondary electron (SE) detector, and backscattered electron (BSE) detector. The SEM is also equipped with an energy dispersive X-ray spectroscopy (EDS) detector enabled for spot, line, and mapping microanalysis. SEM images of the GDE surface and inner structure are captured at various magnifications (100X, 200X and 250X). Both SE and BSE detectors are used for image generation, along with EDS microanalysis for elemental mapping of the precipitates and the electrocatalyst in the GDE structure.

Furthermore, to evaluate the effect of salt deposition on the hydrophobicity/hydrophilicity and wettability of the GDEs, the static water contact angle is measured using the sessile drop method. This measurement is performed with a contact angle measurement system (DSA25, Krüss, Germany), where a 2.0 μL water drop is placed on the surface of different layers at different sites to obtain an average water contact angle value. Image recognition software is used to obtain this value.

**Table 2**
Summary of experimental conditions for evaluating acid anolyte performance in gas-phase $CO_2$ electroreduction to formate.

| Experimental point | $K_2SO_4$ Concentration (M) | pH | Flow rate per geometric surface area (mL $min^{-1}$ $cm^{-2}$) |
|---|---|---|---|
| Anolyte composition | | | |
| 1 | 0.1 | | |
| 2 | 0.2 | | |
| 3 | 0.3 | 2 | 0.57 |
| 4 | 0.4 | | |
| 5 | 0.5 | | |
| Anolyte pH | | | |
| 6 | Best result | 1 | |
| 7 | Best result | 2 | 0.57 |
| 8 | Best result | 3 | |
| 9 | Best result | 4 | |
| Anolyte flow rate per geometric surface area | | | |
| 10 | Best result | | 0.14 |
| 11 | Best result | | 0.28 |
| 12 | Best result | | 0.57 |
| 13 | Best result | | 0.85 |
| 14 | Best result | | 1.14 |
| 15 | Best result | | 1.71 |

### 2.5. Figures of merit

The performance of the electrochemical $CO_2$ reduction to formate is evaluated using the following figures of merit (Eqs. 4–7):

- Faradaic Efficiency, FE, represents the percentage of the current density supplied to the system that is harvested in the production of the target product.

$$FE(\%) = \frac{z \bullet M \bullet F}{j \bullet A} \quad (4)$$

Where $z$ is the number of electrons exchanged during the reduction of $CO_2$ (2 in the case of formate), $M$ is the moles of the target product generated during the experiment duration, $F$ is the Faraday constant (96485 C $mol^{-1}$), $j$ is the applied current density, and $A$ is the geometric area of the reactor.

- Formate rate, indicates the formation of the target product per unit of time and area within the system.

$$Rate\left(\frac{mol}{m^2 \bullet s}\right) = \frac{M}{t \bullet A} \quad (5)$$

Where $M$ and $A$ have the same meaning as in Eq. 4, and t is the duration of each experiment.

- Energy consumption, EC, is defined as the total energy required to produce one kilomole of the target product.

$$EC\left(\frac{kWh}{kmol}\right) = \frac{j \bullet A \bullet V}{M} \quad (6)$$

Where $j$, $A$ and $M$ have the same meaning as in Eqs. 4 and 5, and V is the overall cell potential recorded during each experiment.

- Activity loss: The reduction in GDE performance over time is assessed by approximating the formate rate versus time to a first order deactivation model, as presented in Eq. 7:

$$Formate\ rate(t) = Formate\ rate_0 \bullet e^{(-kd \bullet t)} \quad (7)$$

Where *Formate rate (t)* is the evolution of the reaction rate to formate over time, *Formate rate₀* is the initial reaction rate, *kd* is the deactivation constant and *t* is time. The deactivation constant can be estimated from the experimental data by plotting the logarithm of the formate rate versus time. The adjusted linear slope in this plot corresponds to the deactivation constant *kd*.

## 3. Results

### 3.1. $CO_2$ electrolysis in alkaline conditions

To evaluate the effects of salt precipitation and establish a reference for comparing different gas-phase $CO_2$ electroreduction results, an initial evaluation is proposed using an alkaline anolyte. Specifically, a 1 M KOH (pH 14) solution will be fed into the electrochemical reactor at a constant flow rate of 0.57 mL $min^{-1}$ $cm^{-2}$, while operating at a constant current density of 200 mA $cm^{-2}$. These experimental conditions will remain constant to facilitate comparisons between different anolytes.

The formate concentration obtained reaches 204 g $L^{-1}$, with a FE of 66 %, a formate rate of 6.94 mmol $m^{-2}$ $s^{-1}$, and an EC of 196 kWh $kmol^{-1}$, which are in concordance with previous results obtained under similar experimental conditions [16]. However, the total carbonate and bicarbonate concentration in the collected sample is 1460 g $L^{-1}$, which significantly exceeds the solubility of potassium (bi)carbonates [24], indicating salt precipitation over the cathode. This is evaluated by visual inspection and GDE surface characterization by XRD, as shown in Fig. 2.

As observed in Fig. 2.a, the insoluble salts precipitate on the GDE structure, causing the porous structure to clog, which hinders the $CO_2$

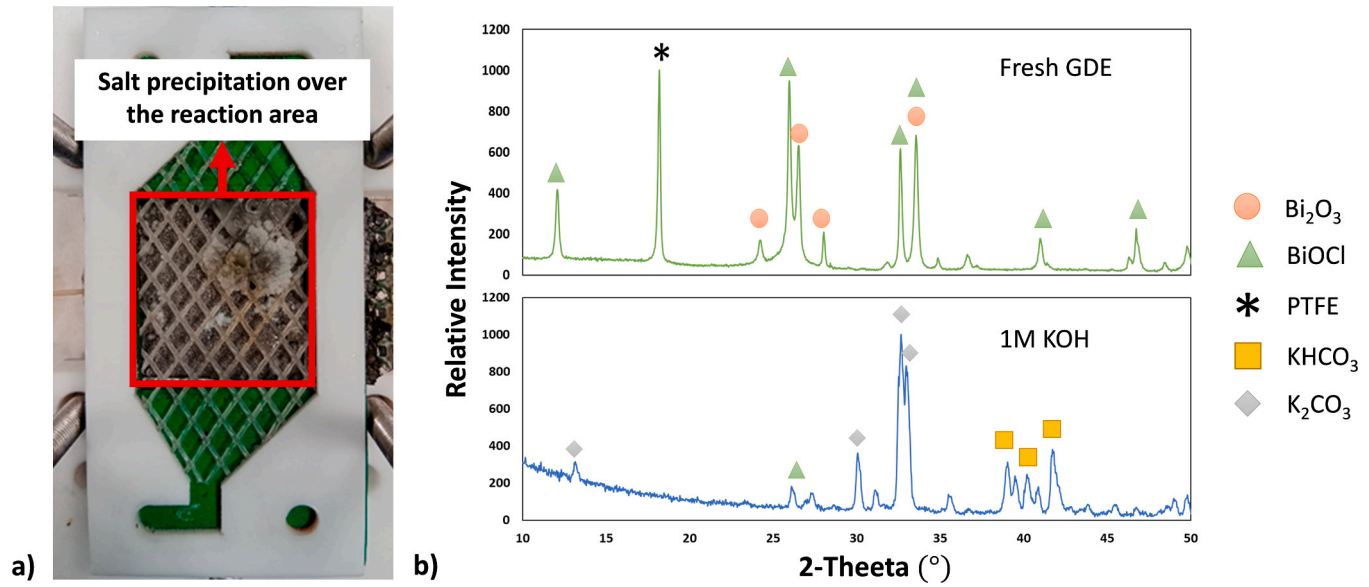


**Fig. 2.** a) Visual identification of salt precipitation on the GDE in the filter-press reactor after 1 h operation and b) Comparison between the XRD diffractograms of the unused GDE and the GDE used under alkaline conditions (1 M KOH).

access to the reaction sites and increases the mass transfer resistance for both $CO_2$ and reaction products like formate. This leads to the rapid deactivation of the GDE [25,28]. Moreover, the XRD diffractograms (Fig. 2.b) confirm the deposition of potassium carbonate and potassium bicarbonate on the GDE surface, covering the Bismuth species and PTFE present on the GDE surface. This assessment is made by comparing the diffractograms of both the fresh GDE and the GDE used with 1 M KOH.

It is worth noting the composition of the unused GDE, as expected, PTFE and $Bi_2O_3$ appear, and additionally, BiOCl is detected. The appearance of this Bi-based compound could be attributed to its formation during the GDE activation with 1 M HCl. The hypothesis of (bi) carbonate deposition is further confirmed by the SEM imaging and EDS mapping analysis presented in Fig. 3.

In Fig. 3, we observe that the fresh GDE exhibits a smooth and uniform surface with the Bi-based catalyst distributed throughout. The cross-sectional SEM image and EDS mapping show that the catalyst (Bi-based) is dispersed across the porous structure of the GDE, providing a significant surface area for $CO_2$ access to the catalyst's active sites. In both cases, the EDS mapping does not detect the presence of potassium.

Upon usage in alkaline conditions (1 M KOH) for 1 hour, the surface of the GDE develops pronounced irregularities due to the presence of potassium (bi)carbonates, which coat the entire surface, as indicated by the EDS mapping. Additionally, the cross-sectional EDS mapping reveals that the salts not only accumulate on the surface but also infiltrate the GDE structure, clogging the pores. This salt precipitation affects the thickness of the GDE, increasing it significantly from 290 to 450 μm after use. The augmented thickness could result in higher $CO_2$ mass transfer resistance [40]. Moreover, the salt precipitation covering the catalyst active sites and blocking the pores impairs the GDE performance, representing one of the primary mechanisms for rapid [41].

### 3.2. *$CO_2$ electrolysis with acid anolyte: Electrolyte composition*

As demonstrated, $CO_2$ electroreduction to formate using highly alkaline media as anolyte (1 M KOH) presents a significant issue: salt precipitation on the GDE structure, which rapidly affects the system operation as the electrode loses activity. To mitigate salt precipitation, the use of an acid solution as anolyte is proposed. In this case, $K_2SO_4$ is

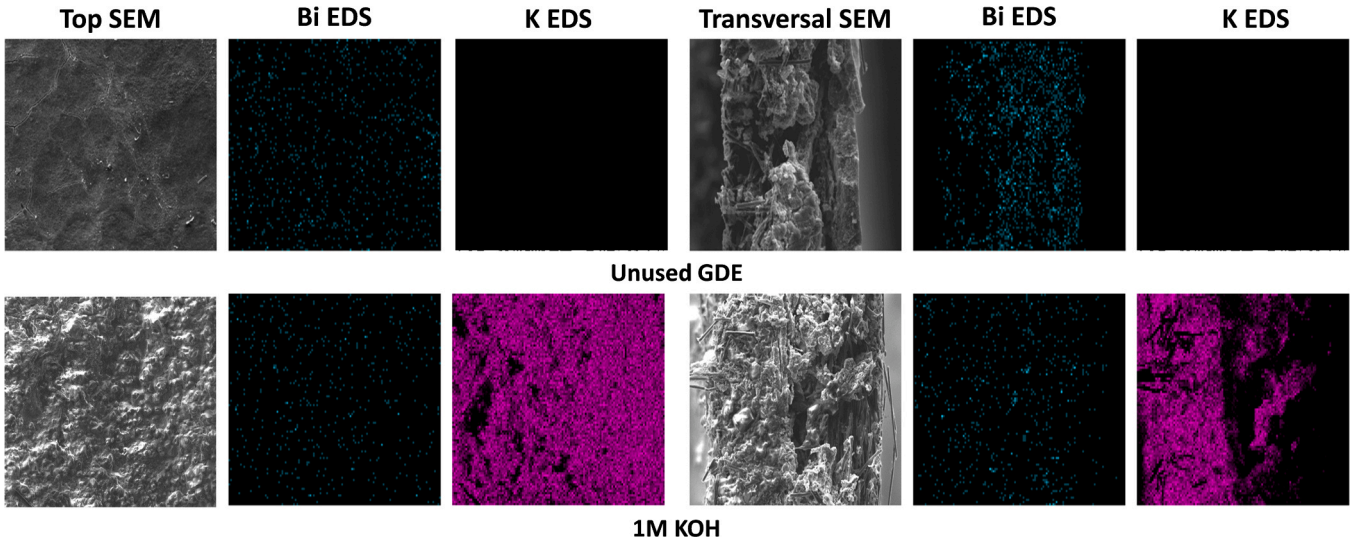


**Fig. 3.** SEM imaging and EDS mapping for the surface and cross-sectional of both the unused GDE and the GDE tested with 1 M KOH.

employed as the solute to ensure conductivity in the anode compartment, while $H_2SO_4$ is added to adjust the pH.

First, the anolyte composition is evaluated using anolytes with concentrations between 0.1 and 0.5 M $K_2SO_4$, at a constant pH 2. The concentration of the solute ($K_2SO_4$) is directly related to the concentration of the metal cations in the anolyte. Higher concentrations of $K^+$ cations increase the concentration gradient, favoring the cations to cross the cation exchange membrane towards the cathode, where they form insoluble salts when combined with carbonate or bicarbonate anions [42]. Therefore, it is important to find a balance between a highly conductive anolyte, which reduces the cell voltage, and avoiding excessive $K^+$ that may form undesirable (bi)carbonates on the GDE cathode.

In Fig. 4, the results for the different figures of merit evaluating the $CO_2$ electroreduction performance to formate at a constant current density of 200 mA $cm^{-2}$ and an anolyte flow rate of 0.57 mL $min^{-1}$ $cm^{-2}$ are presented, along with a visual analysis of the salt precipitation after each experiment.

As seen in Fig. 4.a, the formate concentration increases with higher $K_2SO_4$ concentrations, ranging from 34 g $L^{-1}$ at 0.1 M to 164 g $L^{-1}$ at 0.5 M $K_2SO_4$. The increase in anolyte conductivity may improve the overall $CO_2$ reduction reaction, leading to higher FEs of over 55 %, as shown in Fig. 4.b. However, the total (bi)carbonate concentration in the reactor outlet also increases, reaching 740 g $L^{-1}$ for 0.4 M $K_2SO_4$, which exceeds the solubility limits for potassium carbonate and bicarbonate [24]. This promotes salt precipitation at concentrations above 0.3 M $K_2SO_4$, as observed in Fig. 4.c.

Regarding EC, there is a decrease with more concentrated anolytes, as higher conductivity results in lower cell voltages. Low-concentration anolytes yield EC values over 1200 kWh $kmol^{-1}$, which are reduced to below 350 kWh $kmol^{-1}$ with high-concentration anolytes. The formate rate follows a linear trend (Figure S.2), increasing with higher anolyte concentration, ranging from 1.8 mmol $m^{-2}$ $s^{-1}$ to 6.07 mmol $m^{-2}$ $s^{-1}$. Considering all evaluated aspects, the best compromise between higher FEs (32 %) and formate concentration (68 g $L^{-1}$), while maintaining low EC (522 kWh $kmol^{-1}$) and minimizing salt precipitation (323 g $L^{-1}$), is achieved with the 0.3 M $K_2SO_4$ anolyte at a constant pH of 2.

Besides, different solute concentrations affect the salt precipitation phenomena on the GDE surface and structure. For instance, the hydrophobic behavior of the unused GDEs is affected by the deposition of insoluble salts on their surface [27]. This is assessed by the water contact angle, as presented in Figure S3. GDEs used with anolytes under 0.3 M $K_2SO_4$ concentration maintain some hydrophobicity (approximately 40° contact angle), while the rest become completely hydrophilic as potassium carbonates and bicarbonates cover the surface. The salt precipitation and deposition on the GDE surface and the crystalline phases present when using different anolyte concentrations can be estimated by XRD, as shown in Fig. 5.

When comparing the results shown in Fig. 5 with the diffractogram of the fresh GDE (Fig. 2), it is evident that for the GDE used with 0.1 M $K_2SO_4$, there is no detection of potassium carbonate or bicarbonate. The main changes in the signals are associated with the reduction of $Bi_2O_3$ and BiOCl to metallic Bi under the reaction conditions at the cathode. This transformation is also observed for the GDEs utilized with 0.2 and 0.3 M $K_2SO_4$. According to Bienen et al. [43], this transformation may not affect the electrocatalyst's activity towards formate. Besides, the presence of Bi-based compounds and PTFE is evident for GDEs used with 0.1, 0.2, and 0.3 M $K_2SO_4$, with increased signal intensity of potassium carbonate and bicarbonate in the latter.

In the case of 0.4 and 0.5 M $K_2SO_4$, the signals of the Bi-based catalyst and PTFE are almost obscured by the $K_2CO_3$ and $KHCO_3$, demonstrating the abundant presence of salts on the GDE surface. This observation aligns with the increased hydrophilicity, as indicated by the water contact angle measurements. Furthermore, the salt distribution within the GDE structure might also be influenced by the concentration of the anolyte employed [44]. Therefore, a further microstructural analysis is conducted using SEM imaging and EDS elemental mapping (Fig. 6).

For the SEM surfaces images (Fig. 6), it can be observed that for the

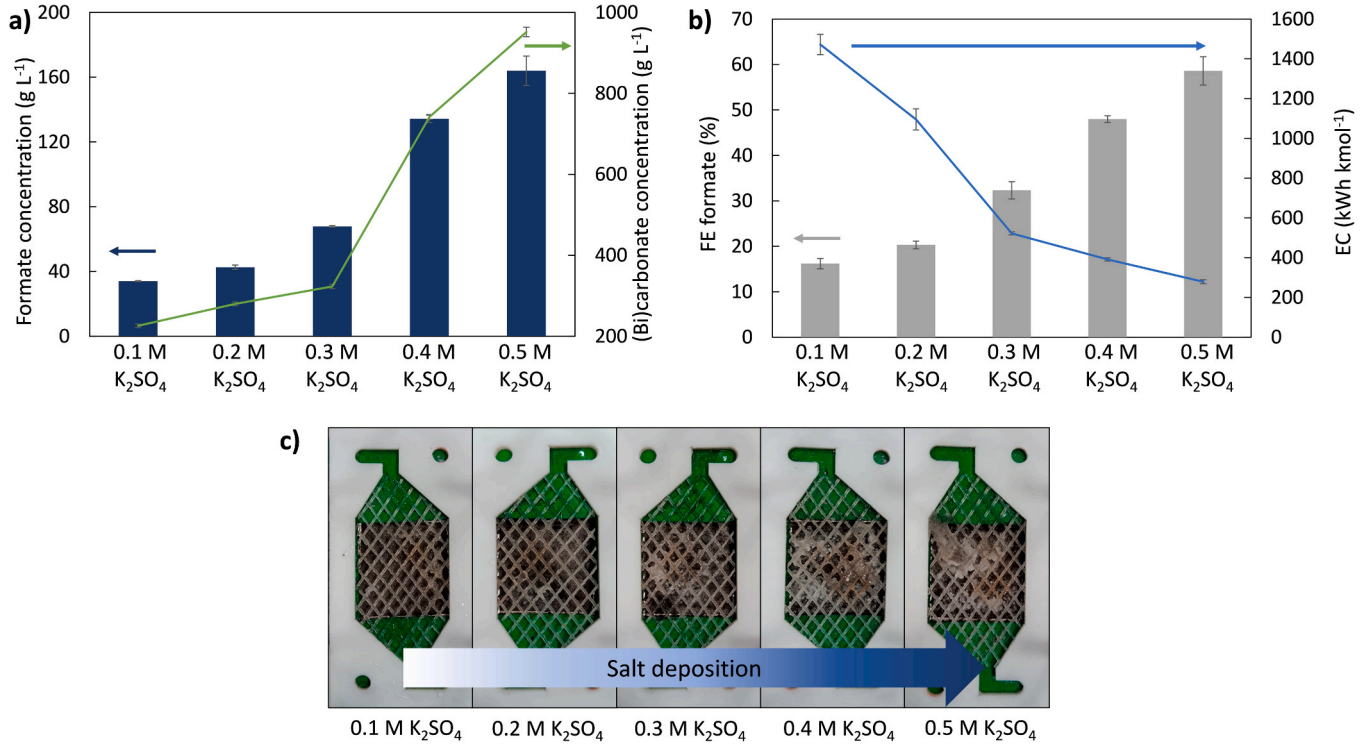


**Fig. 4.** a) Formate concentration and (bi)carbonate concentration, b) Faradaic Efficiency for formate and energy consumption for each anolyte concentration, and c) Visual evaluation of the salt precipitation over the GDE in the electrochemical cell.

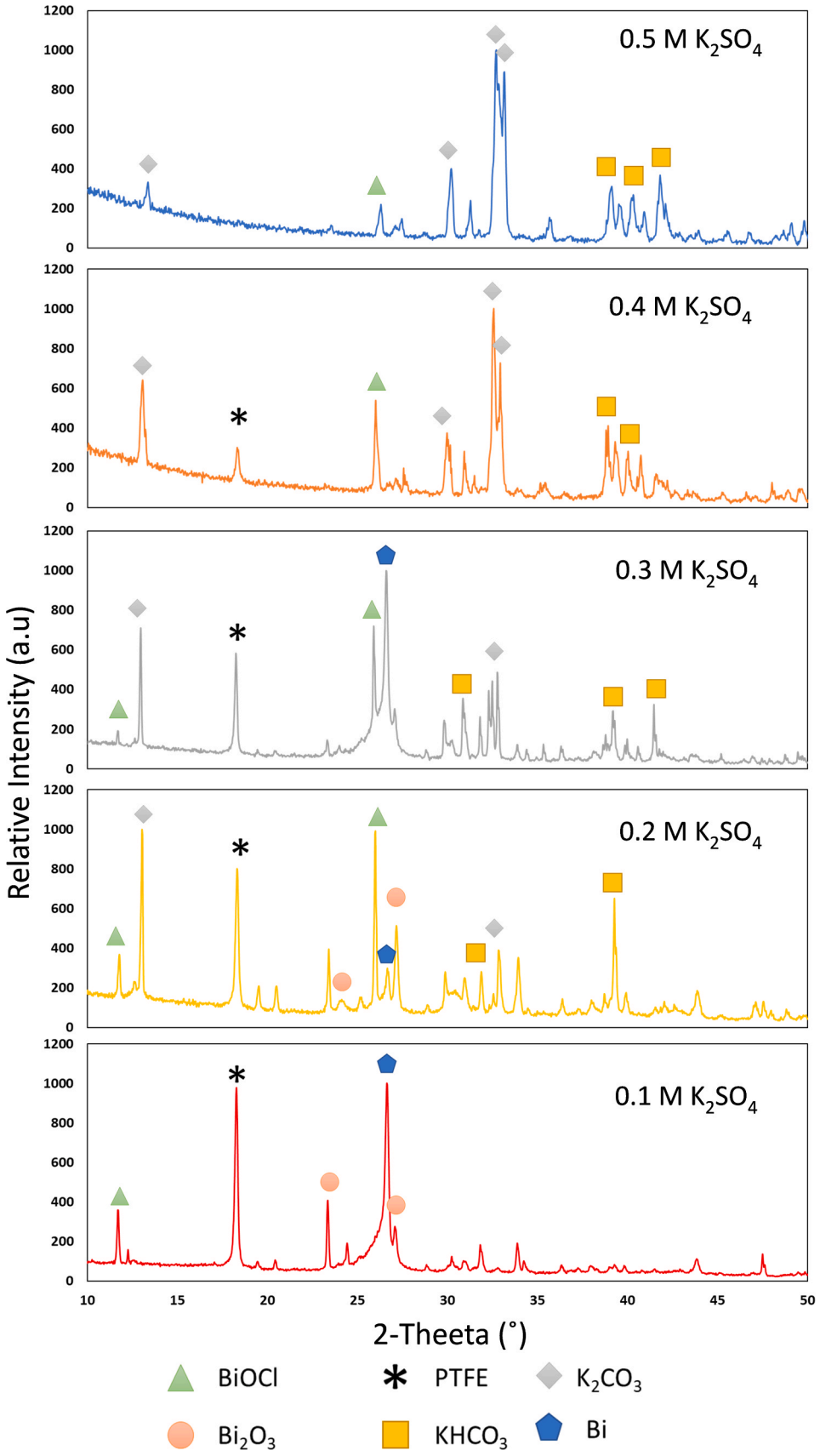


**Fig. 5.** Comparison of the XRD diffractograms and crystalline phases on the GDE surface after a 1 h experiment using different anolyte concentration.

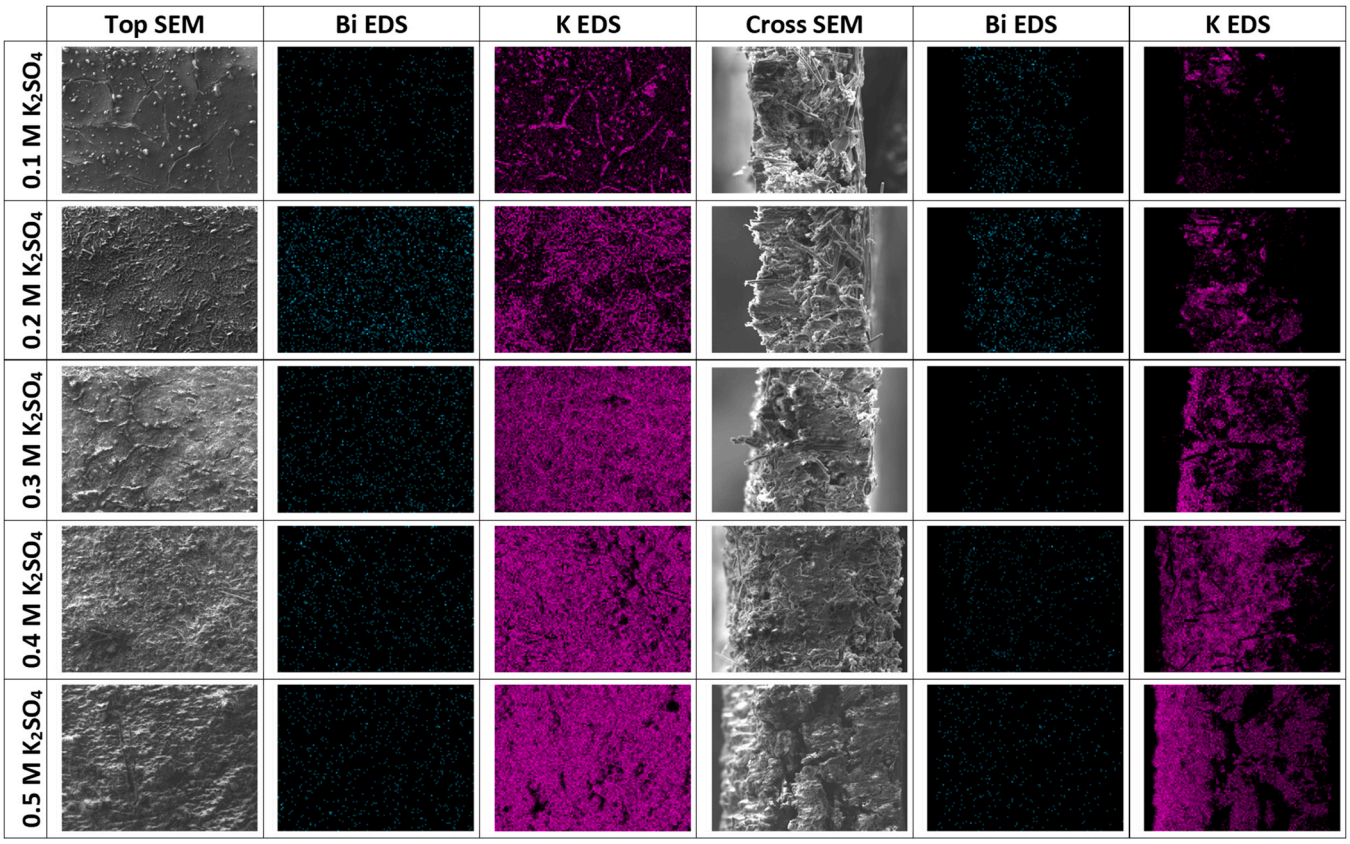


**Fig. 6.** SEM surface and cross-sectional imaging of the GDEs used with different anolyte concentrations and their corresponding EDS elemental mapping for Bismuth and Potassium.

lowest anolyte concentration, 0.1 M $K_2SO_4$, salt formation is very localized, with small crystals appearing on the surface and cracks [45], while the rest of the GDE surface remains smooth. As the concentration of $K_2SO_4$ in the anolyte increases, the surface roughness becomes more pronounced, becoming extremely heterogeneous for the 0.5 M $K_2SO_4$ anolyte. This can be attributed to the formation and deposition of potassium salts, as revealed by the EDS elemental mapping. As the anolyte concentration increased, the mapping images show a greater amount of surface covered by the potassium signal, which becomes increasingly intense for the 0.4 and 0.5 M $K_2SO_4$ cases. The presence of this amount of salt hinders the contact between the membrane and the GDE, increasing the mass transfer resistance for the protons and $CO_2$ to reach the catalyst active sites to form the formate [46].

Besides, the cross-sectional SEM images provide valuable information about how the morphology of the GDE is modified by using different anolyte compositions. For the range between 0.1 and 0.3 M $K_2SO_4$, the GDEs show a similar structure with almost no alterations. This is further supported by the EDS mapping, which shows how potassium is only slightly deposited in the porous structure. In contrast, the GDEs used with 0.4 and 0.5 M $K_2SO_4$ electrolytes show significant alterations in their structure, resulting in an increase in GDE thickness from 285 μm (0.1–0.3 M $K_2SO_4$) to 700 μm (0.5 M $K_2SO_4$). This is mainly due to large deposits of potassium carbonate and bicarbonate generated in the pores of the cross-sectional structure of the GDE, as seen in the EDS elemental mapping images. This thickness enlargement and pore-clogging hinder the stability performance of the GDE, as the $CO_2$ access to the active sites is limited, promoting other reactions, such as HER, in the long term [47].

The best performance balance, considering high FEs and formate concentration along with low EC and (bi)carbonate concentration, is achieved with the 0.3 M $K_2SO_4$ anolyte. However, the microstructural analysis and surface composition evaluation show that there is still some salt formation on the GDE. Although these salt deposits do not completely cover the active sites or substantially modify the GDE structure, further strategies are needed to minimize salt formation. One much strategy involves modifying the pH of the 0.3 M $K_2SO_4$ anolyte to assess its impact on the $CO_2$ electrochemical reduction to formate performance.

### 3.3. *Effect of anolyte pH on $CO_2$ electroreduction and salt precipitation*

Once the most suitable anolyte composition is determined (0.3 M $K_2SO_4$), the formation of carbonate and bicarbonate precipitates is reduced but not completely eliminated. Therefore, pH control emerges as an alternative strategy to mitigate these phenomena. It is important to carefully control the pH in the reaction zone to avoid favoring competitive reactions, such as the HER, over the electroreduction of $CO_2$ to formate[38]. To this end, different pH values between 1 and 4 are tested to determine the optimal pH that maximizes $CO_2$ reduction to formate while minimizing salt precipitation. $H_2SO_4$ is added to acidify the anolyte. Fig. 7 presents the results for different figures of merit for $CO_2$ electrolysis in the gas-phase at a constant current density of 200 mA $cm^{-2}$, along with a visual evaluation of salt precipitation on the GDE.

The pH of the anolyte solution has a clear effect on the $CO_2$ electroreduction performance (Fig. 7.a). For instance, with very acidic electrolytes (pH levels of 1 and 2), the formate concentration obtained is around 68 g $L^{-1}$. In contrast, at less acidic pH levels (3–4), the concentration increases to over 110 g $L^{-1}$. The opposite effect occurs with the formation of carbonate and bicarbonate. as seen in Fig. 7.a. While very acidic pH levels limit their formation, keeping concentrations below the solubility limit (260–330 g $L^{-1}$), pH levels of 3 and 4 lead to higher concentrations, exceeding 800 g $L^{-1}$ and causing the precipitation of these salts. This is visually evident, as shown in Fig. 7.c, where salt deposition on the GDE is more pronounced at higher pH levels.

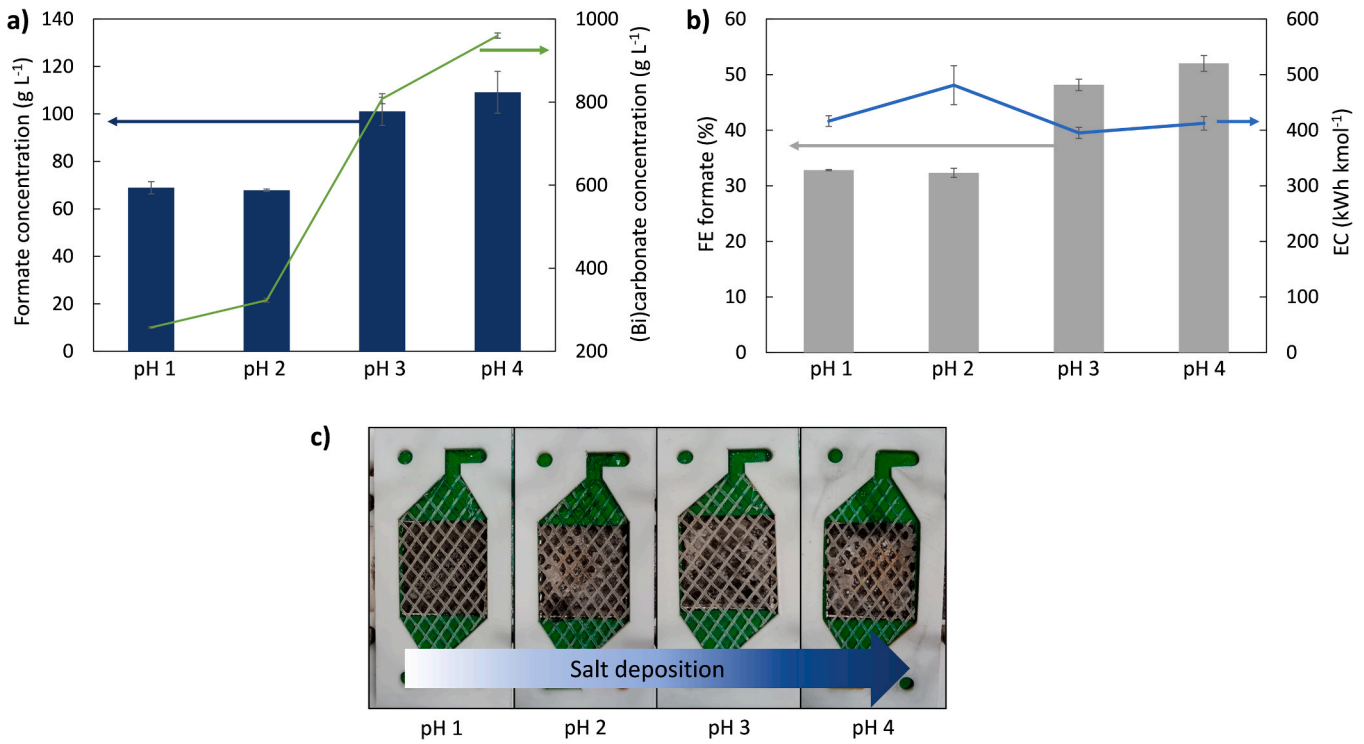


**Fig. 7.** a) Formate concentration and (bi)carbonate concentration, b) Faradaic Efficiency to formate and energy consumption for each pH with 0.3 M $K_2SO_4$ anolyte, and c) Visual evaluation of the salt precipitation on the GDE in the electrochemical cell.

Additionally, the FE follows the same trend as the formate concentration, with pH 1 and 2 showing similar FEs (around 33 %), and pH 3 and 4 increasing the FEs to over 50 % [38]. In terms of EC, pH does not have a clear effect, as the values for each pH are similar. This indicates that the cell voltage is primarily influenced by the solute concentration of the anolyte (0.3 M $K_2SO_4$) rather than the pH value.

In this context, no pH level clearly achieves the balance of high activity in the electroreduction of $CO_2$ to formate and low salt formation on the GDE, as evaluated visually. Therefore, further characterization of the effects of these electrolytes on the GDE is proposed to select the electrolyte that best prevents the precipitation of carbonates and bicarbonates on the cathode by analyzing the physicochemical features of the tested electrodes.

Regarding hydrophobicity, evaluated by the water contact angle after 1 h experiment, it is observed (Figure S.3) that GDEs used with anolytes with pH 1 and 2 maintain a certain hydrophobic character of their surface. In contrast, GDE surfaces employed with less acid anolytes (pH 3–4) become completely hydrophilic. This is due to the formation of carbonate and bicarbonate salts on the GDE surface [47]. This phenomenon is also observed when analyzing the crystal phases on the used GDE surfaces through XRD analysis (Fig. 8).

XRD diffractogram results (Fig. 8) clearly show the presence of potassium carbonate and bicarbonate on the GDE surface when operating with anolytes less acid than pH 2. This salt formation intensifies with increasing pH, gradually obscuring the signals of the Bi-based catalyst. Notably, the potassium carbonate ($K_2CO_3$) signal appears more pronounced than potassium bicarbonate ($KHCO_3$), suggesting its predominance on the GDE surface. Among the tested anolytes, only pH 1 effectively prevents the formation of salt precipitates on the GDE surface. The XRD pattern detects different forms of the Bi-based catalyst, indicating reduction from $Bi_2O_3$ and BiOCl to metallic Bi under the reaction conditions [43]. Furthermore, as previously evaluated, salt precipitation occurs not only on the GDE surface but also throughout its porous structure. To analyze the microstructural changes in the GDE used under different pH anolytes, SEM imaging analysis and EDS mapping are employed, as depicted in Fig. 9.

For pH 1, the GDE keeps a smooth surface after utilization, with few salt crystals appearing in localized areas but without significant accumulation that could affect or clog the surface pores. Cross-sectional analysis shows similar results, with thickness and porous structure remaining largely unchanged compared to the fresh electrode (Fig. 2), and EDS mapping localized spots where salts may have formed, without significantly affecting the porous structure. However, as pH increases, so do irregularities on the electrode surface due to salt precipitation, as evidenced by the EDS mapping, with higher color intensity and greater surface coverage observed at higher pH values. The cross-sectional structure also undergoes significant changes, with clear thickening of the electrodes as pH increases, along with increased salt accumulation in the pores, leading to decreased porosity and almost continuous structure at pH 3–4 due to salt accumulation.

Among the evaluated anolyte pH conditions, pH 1 effectively inhibits salt precipitation over the GDE, enhancing electrode stability by preventing pore blockage and maintaining a high volumetric area available for $CO_2$ access to the catalyst's active sites. This facilitates efficient product evacuation by avoiding additional material, as the transfer resistance caused by salt accumulation. Using pH 1 and 0.3 M $K_2SO_4$ anolyte, the $CO_2$ electrolysis performance achieves a formate concentration of 68 g $L^{-1}$, with a FE of 33 %, formate rate of 1.68 mmol $m^{-2}$ $s^{-1}$, and an EC of 416 kWh $kmol^{-1}$. Thus, the system performance can be further optimized by modifying the anolyte flow rate to improve OER coupling with $CO_2$ electroreduction reaction.

### 3.4. *Influence of anolyte flowrate in the $CO_2$ electroreduction to formate*

After determining the optimal anolyte composition and pH (0.3 M $K_2SO_4$, pH 1) to avoid salt precipitation on the GDE cathode while maintaining excellent performance for $CO_2$ electrolysis toward formate, the influence of the anolyte flow per geometric area is assessed. Different flow rates, ranging from 0.14–1.71 mL $min^{-1}$ $cm^{-2}$ are tested to evaluate their impact on $CO_2$ electroreduction performance, finding an

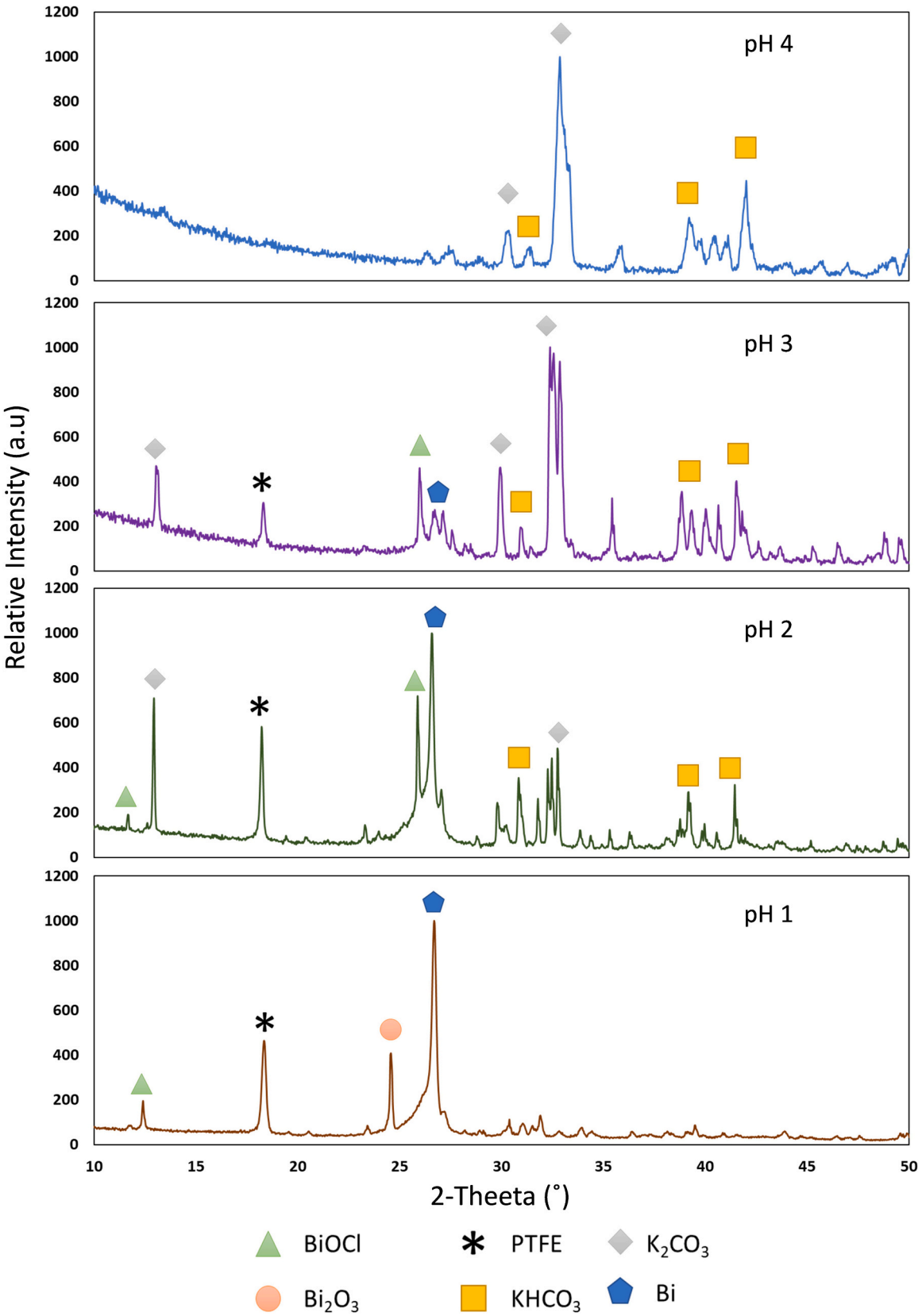


**Fig. 8.** Comparison of XRD diffractograms and crystalline phases for the GDE surface after 1 h experiment using anolytes with different pH values but the same composition (0.3 M $K_2SO_4$).

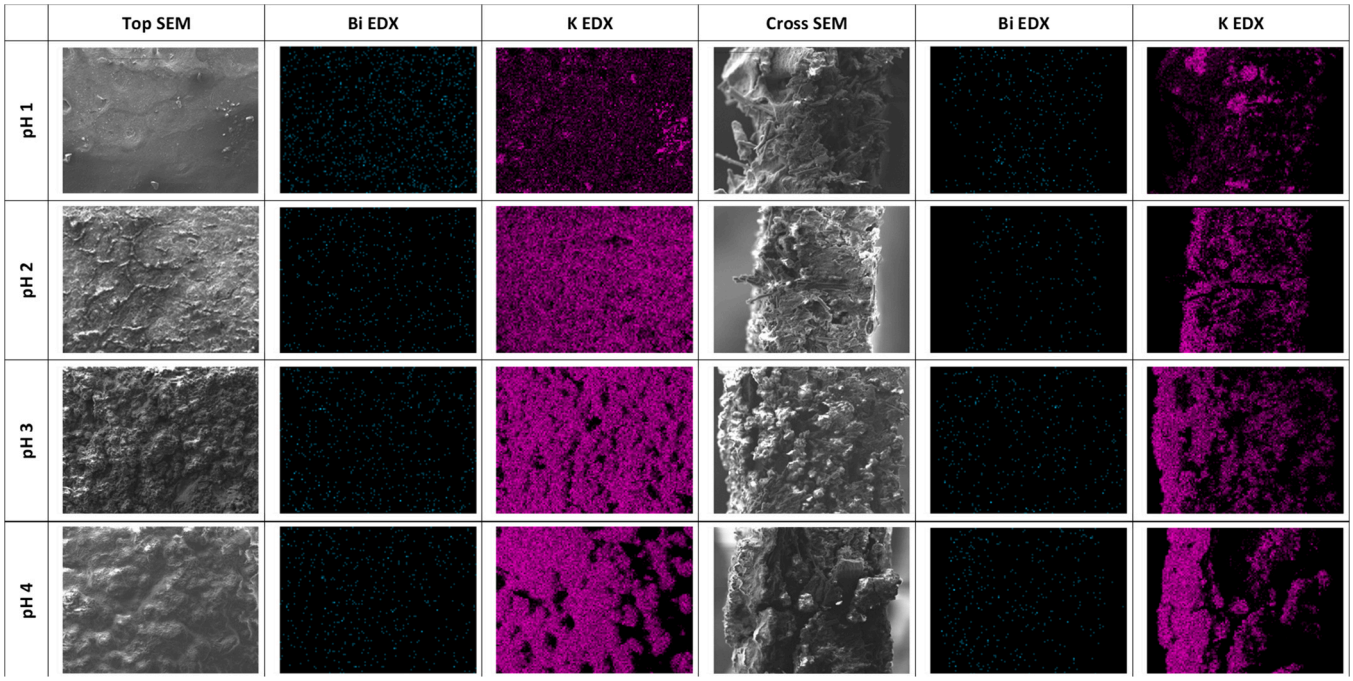


**Fig. 9.** SEM surface and cross-sectional imaging of the different GDEs used with different anolyte (0.3 M $K_2SO_4$) pH levels and their corresponding Bismuth and Potassium EDS elemental mapping.

optimal that maximizes both formate production and FE to formate, while minimizing EC and salt formation. Fig. 10 presents the results for the different figures of merit analyzed, operating at a constant current density of 200 mA $cm^{-2}$.

The system performance reaches a maximum value of formate production for an anolyte flow per geometric area of 0.85 mL $min^{-1}$ $cm^{-2}$, with a formate concentration obtained of 87.8 g $L^{-1}$ (Fig. 10.b), and FE to formate of 42 % (Fig. 10.a). Besides, the energy consumption is minimized, 358 kWh $kmol^{-1}$, achieving a reduction of 14 % compared to the reference value with a flow of 0.57 mL $min^{-1}$ $cm^{-2}$. Operating with either very low or high flow rates hinders the electrochemical performance, as observed for anolyte flow rates of 0.14 and 1.71 mL $min^{-1}$ $cm^{-2}$, while intermediate values are optimal, as previously reported [48]. Furthermore, salt precipitation is avoided in all

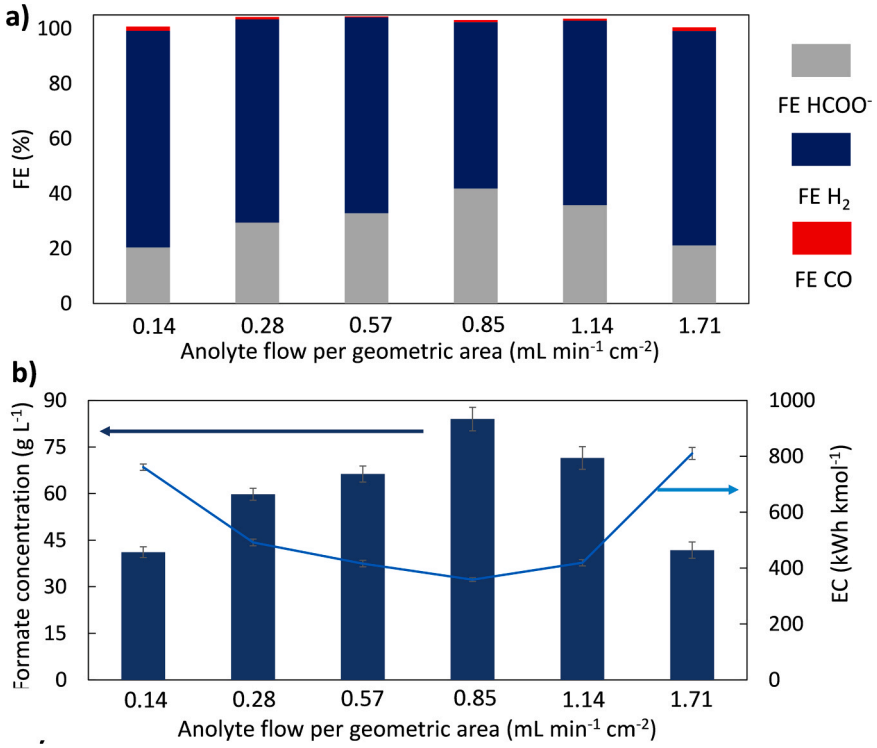


**Fig. 10.** Influence of anolyte flow per geometric area on a) FE for formate ($HCOO^-$), hydrogen ($H_2$), and carbon monoxide (CO), and b) formate concentration and energy consumption. Operating at 200 mA $cm^{-2}$ with an anolyte composition of 0.3 M $K_2SO_4$ and pH 1.

cases, indicating that this phenomenon is more influenced by the anolyte composition and pH. The (bi)carbonate concentration in the reactor outlet remains constant at around 250 g $L^{-1}$, below the solubility limit for both potassium carbonate and bicarbonate.

### 3.5. GDE deactivation in log-term operation

Besides, the optimal operation condition, that maximizes the FE and formate concentration while inhibiting salt precipitation involve using a 0.3 M $K_2SO_4$ anolyte at pH 1 with a flow rate per geometric area of 0.85 mL $min^{-1}$. Under these conditions, a 5-hour experiment is conducted to evaluate the deactivation of the GDE. These results are compared with the $CO_2$ reduction to formate using an alkaline anolyte, 1 M KOH over the same duration of 5 hours. The experimental conditions for both cases are identical: current density of 200 mA $cm^{-2}$, a continuous supply of humified $CO_2$ at 200 mL $min^{-1}$, and a GDE with a catalyst loading of 4 mg $cm^{-2}$. Fig. 11 presents a comparison between the FE and formate concentration, with samples taken each hour.

Initially, the performance of the $CO_2$ electroreduction system using an alkaline anolyte is superior to that using an acidic anolyte. In alkaline conditions, the formate concentration achieved is much higher, while the FE remains similar. This is expected, as alkaline conditions favor the reaction selectivity and rate towards the formate formation [5]. Nevertheless, the activity of the 1 M KOH $CO_2$ electroreduction system rapidly declines as insoluble salts start to deposit on the GDE structure, provoking a fast deactivation. Both FE and formate concentration dropped by more than 50 % by the second hour of the experiment. The activity loss continues until the end of the 5-hour test, with an overall reduction of FE from 44 % to 3 % and formate concentration from 222 to 15 g $L^{-1}$.

On the other hand, using the acid anolyte (0.3 M $K_2SO_4$, pH 1), the initial activity is much lower compared to the alkaline media, with formate concentrations around 90 g $L^{-1}$, and an FE of 42 %. However, there is no significant activity loss during the first 3 hours of the experiment, as the initial GDE deactivation method (salt precipitation) is inhibited. The activity loss during these first 3 hours is less than 10 %, demonstrating a more stable behavior compared to the alkaline anolyte, which experiences performance losses of over 90 % in the same period. Thus, the hydrophobicity of the GDE is affected during the stability tests employing the acidic anolyte, as there is a significant reduction in the water contact angle from 95° in the first hour to 28° at the end of 5 hours. This behavior can be related to a phenomenon previously described in the literature when using acidic electrolytes [49–51]. The high concentration of $K^+$ cations in the anolyte migrates through the membrane to the cathode and accumulates in the reaction zone over time. This $K^+$ accumulation increases the pH near the electrode surface, evolving from acidic to neutral or slightly alkaline media, thus promoting the formation of carbonate and bicarbonate salts [49], which might be behind the reduction in the hydrophobicity over the GDE surface after 5 hours of testing. Nevertheless, during the experimental period, no salt precipitate was observed in the reaction zone. By the end of the 5-hour test, there is a decrease in GDE activity, likely due to the increase of pH in the reaction zone, favoring the carbonate and bicarbonate formation, or other deactivation mechanisms occurring over longer periods, such as electrochemical wetting of the electrode or catalyst leaching [20,52].

Deactivation is observed under both experimental conditions (Fig. 11), though it occurs differently in each case. To evaluate the rate of GDE deactivation in each condition, a first-order deactivation constant is estimated [53]. The formate rate evolution over time is approximated to a first-order deactivation function (Eq. 7). By plotting the logarithm of the formate rate versus time, the deactivation constant is estimated (Fig. 12). For each experimental condition, the data points considered are those where a decrease in activity is observed: during the first 4 hours for the 1 M KOH, and during the final 3 hours of the experiment for the 0.3 M $K_2SO_4$ at pH 1.

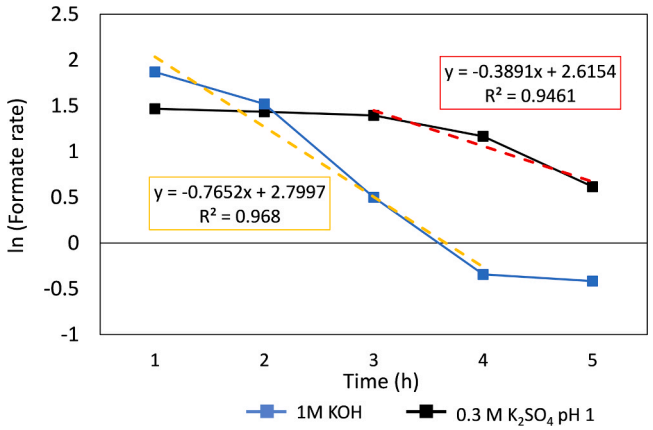


**Fig. 12.** GDE deactivation constant estimation for both anolytes: 1 M KOH and 0.3 M $K_2SO_4$, pH 1.

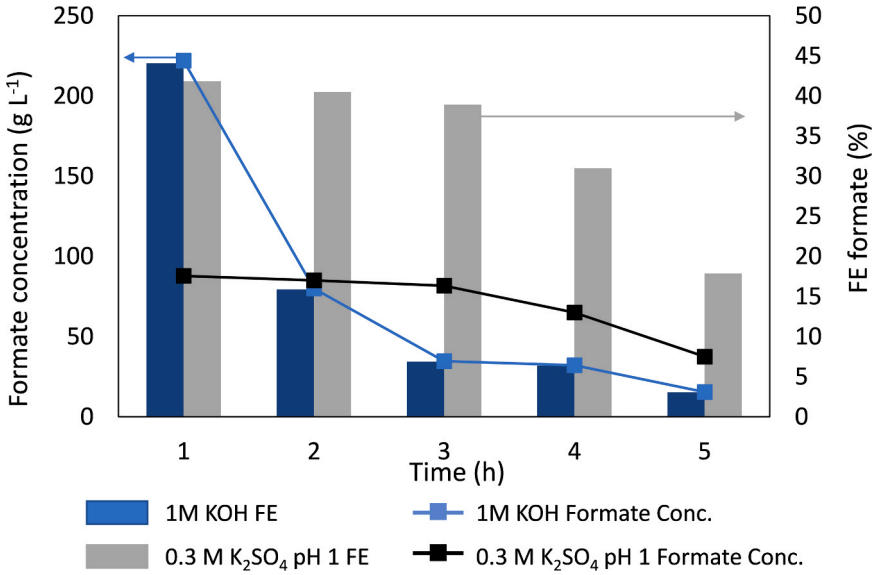


**Fig. 11.** Formate concentration and FE evolution for 5 hours experiment using different anolytes, 1 M KOH and 0.3 M $K_2SO_4$ (pH 1).

The slope of the fitted data is used to estimate the deactivation constant for each case. As observed, the deactivation constant for the GDE using 1 M KOH (0.7652) is more than twice as high as the constant for GDE using the acidic medium (0.3891). This indicates that salt precipitation on the GDE, due to the use of alkaline conditions, occurs much faster than other deactivation mechanisms that may arise during longer operations when salt precipitation is inhibited, as in the case of using 0.3 M $K_2SO_4$ pH 1.

Therefore, in this work, the effect of insoluble salt precipitation on the structure of the GDE has been avoided. This precipitation is the first deactivation mechanism to appear and it affects the electrode more rapidly due to its higher deactivation constant. However, even when this mechanism is inhibited, other types of activity losses are observed in long-term experiments. These losses can be attributed to phenomena such as electrochemical wetting of the GDE, which floods the pores of its structure, or the detachment of the catalyst deposited on the GDE [52].

It is thus necessary to continue studying these deactivation mechanisms to achieve stable operations lasting tens of hours in the electroreduction of $CO_2$ to formate in the gas phase, thereby enabling the scale-up and industrial implementation of this technology.

## 4. Conclusions

The formation and precipitation of carbonates and bicarbonates over the GDE represent significant activity loss mechanisms, particularly detrimental in alkaline conditions for the $CO_2$ electroreduction to formate. This issue is exacerbated when using a in gas phase systems where the absence of a liquid catholyte allows for easy precipitation of insoluble salts upon reaching the solubility limit. Experimentation with 1 M KOH revealed complete coverage of the GDE surface and pore blockage by potassium carbonates and bicarbonates, hindering $CO_2$ access to the reaction zone and catalyst active sites.

To address this, the use of acid anolytes to limit salt precipitation is proposed. Anolyte composition, specifically the concentration of solute ($K_2SO_4$), is evaluated to achieve high yields of $CO_2$ electroreduction to formate and minimize salt precipitation. Optimal conditions are found with 0.3 M $K_2SO_4$ at pH 2, yielding 68 g $L^{-1}$ of formate and 32 % FE, while reducing salt formation as confirmed by XRD, SEM, and EDS analysis. Physicochemical characterization revealed that pH 1–2 anolytes effectively prevented salt precipitation, unlike pH 3–4 solutions, which led to pore-clogging salt formations.

Upon determining the optimal anolyte, optimizing the operational conditions such as flowrate per geometric area are optimized. It was found that this parameter did not influence carbonate and bicarbonate formation, with a peak performance observed at a flow rate of 0.85 mL $min^{-1}$ $cm^{-2}$ flowrate, resulting in 88 g $L^{-1}$ of formate concentration, FE of 42 % and 358 kWh kmol-1 of EC. The predominant byproducts generated were $H_2$ (58 % FE) and CO (0.7 % FE).

Long-term experiments comparing alkaline anolyte (1 M KOH) and acidic (0.3 M $K_2SO_4$ pH 1) anolytes revealed rapid GDE deactivation under alkaline conditions (deactivation constant: 0.7652), with over 90 % performance loss within hours. In contrast, GDEs operated with acid anolytes showed stable performance for the initial 3 hours followed by a gradual deactivation (deactivation constant: 0.3891) without salt precipitation.

All in all, the use of acidic anolytes shows promise in mitigating carbonate and bicarbonate precipitation, enabling prolonged operation in gas-phase $CO_2$ reduction to formate. However, selectivity towards formate is compromised, necessitating further research into catalyst and electrode designs. Additionally, despite mitigating salt precipitation, other activity loss phenomena emerge during long-term operation, warranting efforts towards more robust GDEs and precise control of reaction conditions for sustained operation over extended periods.

## CRediT authorship contribution statement

**Angel Irabien:** Writing – review & editing, Resources, Project administration, Funding acquisition, Formal analysis. **Guillermo Díaz-Sainz:** Writing – review & editing, Supervision, Project administration, Funding acquisition, Formal analysis, Conceptualization. **Jose Antonio Abarca:** Writing – original draft, Methodology, Investigation, Data curation, Conceptualization.

## Declaration of Competing Interest

The authors declare that they have no known competing financial interests or personal relationships that could have appeared to influence the work reported in this paper.

## Data Availability

Data will be made available on request.

## Acknowledgments

The authors fully acknowledge the financial support received from the Spanish State Research Agency (AEI) through the projects PID2020-112845RB-I00, TED2021-129810B-C21, and PLEC2022-009398 (MCIN/AEI/10.13039/501100011033 and Union Europea Next Generation EU/PRTR). The present work is related to CAPTUS Project. This project has received funding from the European Union's Horizon Europe research and innovation programme under grant agreement No 101118265.". Jose Antonio Abarca gratefully acknowledges the predoctoral research grant (FPI) PRE2021-097200.

## Appendix A. Supporting information

Supplementary data associated with this article can be found in the online version at doi:10.1016/j.jcou.2024.102897.

## References

[1] US EPA. Global Greenhouse Gas Overview. https://www.epa.gov/ghgemissions/global-greenhouse-gas-overview, 2024 (Accessed 29 May 2024)
[2] COP28. Net-Zero Transition Charter. https://www.cop28.com/en/net-zero-accountability-charter, 2024 (Accessed 29 May 2024)
[3] A.I. Osman, M. Hefny, M.I.A. Abdel Maksoud, A.M. Elgarahy, D.W. Rooney, Environ. Chem. Lett. 19 (2021) 797–849.
[4] D. Xu, K. Li, B. Jia, W. Sun, W. Zhang, X. Liu, T. Ma, Carbon Energy 5 (2023) e230.
[5] K. Fernández-Caso, G. Díaz-Sainz, M. Alvarez-Guerra, A. Irabien, ACS Energy Lett. 8 (2023) 1992–2024.
[6] Y.Y. Birdja, E. Pérez-Gallent, M.C. Figueiredo, A.J. Göttle, F. Calle-Vallejo, M.T. M. Koper, Nat. Energy 4 (2019) 732–745.
[7] M. Rumayor, A. Dominguez-Ramos, P. Perez, A. Irabien, J. $CO_2$ Util. 34 (2019) 490–499.
[8] G. Díaz-Sainz, M. Alvarez-Guerra, A. Irabien, Molecules 25 (2020) 4457.
[9] G. Díaz-Sainz, M. Alvarez-Guerra, J. Solla-Gullón, L. García-Cruz, V. Montiel, A. Irabien, Catal. Today 346 (2020) 58–64.
[10] S. Zhang, Q. Fan, R. Xia, T.J. Meyer, Acc. Chem. Res. 53 (2020) 255–264.
[11] G. Díaz-Sainz, M. Alvarez-Guerra, A. Irabien, J. $CO_2$ Util. 56 (2022) 101822.
[12] G. Díaz-Sainz, M. Alvarez-Guerra, J. Solla-Gullón, L. García-Cruz, V. Montiel, A. Irabien, AIChE J. 66 (2020) e16299.
[13] Y. Kang, T. Kim, K.Y. Jung, K.T. Park, Catal 13 (2023) 955.
[14] J. Antonio Abarca, G. Díaz-Sainz, I. Merino-Garcia, A. Irabien, J. Albo, J. Energy Chem. 85 (2023) 455–480.
[15] J.A. Abarca, G. Díaz-Sainz, I. Merino-Garcia, G. Beobide, J. Albo, A. Irabien, J. Environ. Chem. Eng. (2023) 109724.
[16] G. Díaz-Sainz, M. Alvarez-Guerra, B. Ávila-Bolívar, J. Solla-Gullón, V. Montiel, A. Irabien, Chem. Eng. J. 405 (2021) 126965.
[17] G. Díaz-Sainz, J.A. Abarca, M. Alvarez-Guerra, A. Irabien, J. $CO_2$ Util. 81 (2024) 102735.
[18] P. Zhu, H. Wang, Nat. Catal. 4 (2021) 943–951.
[19] T. Moore, X. Xia, S.E. Baker, E.B. Duoss, V.A. Beck, ACS Energy Lett. 6 (2021) 3600–3606.
[20] H. Rabiee, L. Ge, X. Zhang, S. Hu, M. Li, Z. Yuan, Energy Environ. Sci. 14 (2021) 1959–2008.

[21] C.P. O'Brien, R.K. Miao, S. Liu, Y. Xu, G. Lee, A. Robb, J.E. Huang, K. Xie, K. Bertens, C.M. Gabardo, J.P. Edwards, C.T. Dinh, E.H. Sargent, D. Sinton, ACS Energy Lett. 6 (2021) 2952–2959.
[22] D. Du, R. Lan, J. Humphreys, S. Tao, J. Appl. Electrochem. 47 (2017) 661–678.
[23] E.R. Cofell, U.O. Nwabara, S.S. Bhargava, D.E. Henckel, P.J.A. Kenis, ACS Appl. Mater. Interfaces 13 (2021) 15132–15142.
[24] J. Disch, L. Bohn, L. Metzler, S. Vierrath, J. Mater. Chem. A Mater. 11 (2023) 7344–7357.
[25] Y. Xu, J.P. Edwards, S. Liu, R.K. Miao, J.E. Huang, C.M. Gabardo, C.P. O'Brien, J. Li, E.H. Sargent, D. Sinton, ACS Energy Lett. 6 (2021) 809–815.
[26] S. Garg, M. Li, A.Z. Weber, L. Ge, L. Li, V. Rudolph, G. Wang, T.E. Rufford, J. Mater. Chem. A Mater. 8 (2020) 1511–1544.
[27] M. Li, M.N. Idros, Y. Wu, T. Burdyny, S. Garg, X.S. Zhao, G. Wang, T.E. Rufford, J. Mater. Chem. A Mater. 9 (2021) 19369–19409.
[28] S. Park, D.T. Wijaya, J. Na, C.W. Lee, Catal 11 (2021) 253.
[29] D.G. Wheeler, B.A.W. Mowbray, A. Reyes, F. Habibzadeh, J. He, C.P. Berlinguette, Energy Environ. Sci. 13 (2020) 5126–5134.
[30] B. Endrődi, E. Kecsenovity, A. Samu, F. Darvas, R.V. Jones, V. Török, A. Danyi, C. Janáky, ACS Energy Lett. 4 (2019) 1770–1777.
[31] S. Verma, Y. Hamasaki, C. Kim, W. Huang, S. Lu, H.R.M. Jhong, A.A. Gewirth, T. Fujigaya, N. Nakashima, P.J.A. Kenis, ACS Energy Lett. 3 (2018) 193–198.
[32] B. De Mot, M. Ramdin, J. Hereijgers, T.J.H. Vlugt, T. Breugelmans, ChemElectroChem 7 (2020) 3839–3843.
[33] D.A. Salvatore, C.M. Gabardo, A. Reyes, C.P. O'Brien, S. Holdcroft, P. Pintauro, B. Bahar, M. Hickner, C. Bae, D. Sinton, E.H. Sargent, C.P. Berlinguette, Nat. Energy 6 (2021) 339–348.
[34] M.A. Blommaert, R. Sharifian, N.U. Shah, N.T. Nesbitt, W.A. Smith, D.A. Vermaas, J. Mater. Chem. A Mater. 9 (2021) 11179–11186.
[35] S.S. Bhargava, E.R. Cofell, P. Chumble, D. Azmoodeh, S. Someshwar, P.J.A. Kenis, Electrochim. Acta 394 (2021) 139055.
[36] X. Li, P. Zhang, L. Zhang, G. Zhang, H. Gao, Z. Pang, J. Yu, C. Pei, T. Wang, J. Gong, Chem. Sci. 14 (2023) 5602–5607.
[37] J. Gu, S. Liu, W. Ni, W. Ren, S. Haussener, X. Hu, Nat. Catal. 5 (2022) 268–276.
[38] W. Wu, L. Xu, Q. Lu, J. Sun, Z. Xu, C. Song, J.C. Yu, Y. Wang, Adv. Mat. (2024) 2312894.
[39] H. Yang, J.J. Kaczur, S.D. Sajjad, R.I. Masel, J. $CO_2$ Util. 20 (2017) 208–217.
[40] Z. Xing, X. Hu, X. Feng, ACS Energy Lett. 6 (2021) 1694–1702.
[41] M. Sassenburg, M. Kelly, S. Subramanian, W.A. Smith, T. Burdyny, ACS Energy Lett. 8 (2023) 321–331.
[42] K.M. Vetter, J. Härtl, D. Reinisch, T. Reichbauer, N. Martić, K.O. Hinrichsen, G. Schmid, ChemElectroChem 9 (2022) e202101165.
[43] F. Bienen, A. Löwe, J. Hildebrand, S. Hertle, D. Schonvogel, D. Kopljar, N. Wagner, E. Klemm, K.A. Friedrich, J. Energy Chem. 62 (2021) 367–376.
[44] B. Endrődi, A. Samu, E. Kecsenovity, T. Halmágyi, D. Sebők, C. Janáky, Nat. Energy 6 (2021) 439–448.
[45] H. Hu, Y. Kong, M. Liu, V. Kolivoška, A.V. Rudnev, Y. Hou, R. Erni, S. Vesztergom, P. Broekmann, J. Mater. Chem. A Mater. 11 (2022) 5083–5094.
[46] L.C. Weng, A.T. Bell, A.Z. Weber, Energy Environ. Sci. 12 (2019) 1950–1968.
[47] A.B. Moss, S. Garg, M. Mirolo, C.A. Giron Rodriguez, R. Ilvonen, I. Chorkendorff, J. Drnec, B. Seger, Joule 7 (2023) 350–365.
[48] G. Díaz-Sainz, K. Fernández-Caso, T. Lagarteira, S. Delgado, M. Alvarez-Guerra, A. Mendes, A. Irabien, J. Environ. Chem. Eng. 11 (2023) 109171.
[49] J.E. Huang, F. Li, A. Ozden, A.S. Rasouli, F.P.G. de Arquer, S. Liu, S. Zhang, M. Luo, X. Wang, Y. Lum, Y. Xu, K. Bertens, R.K. Miao, C.T. Dinh, D. Sinton, E.H. Sargent, Sci 372 (2021) 1074–1078.
[50] M. Fan, J.E. Huang, R.K. Miao, Y. Mao, P. Ou, F. Li, X.Y. Li, Y. Cao, Z. Zhang, J. Zhang, Y. Yan, A. Ozden, W. Ni, Y. Wang, Y. Zhao, Z. Chen, B. Khatir, C. P. O'Brien, Y. Xu, Y.C. Xiao, G.I.N. Waterhouse, K. Golovin, Z. Wang, E.H. Sargent, D. Sinton, Nat. Cat. 6 (2023) 763–772.
[51] H.G. Qin, Y.F. Du, Y.Y. Bai, F.Z. Li, X. Yue, H. Wang, J.Z. Peng, J. Gu, Nat. Commun. 14 (2023) 1–10.
[52] T.N. Nguyen, C.T. Dinh, Chem. Soc. Rev. 49 (2020) 7488–7504.
[53] Z.M. Shakor, E.N. Al-Shafei, RSC Adv. 13 (2023) 22579.